BIOCHEMISTRY

Self-folding of supramolecular polymers into bioinspired topology

Deepak D. Prabhu[1], Keisuke Aratsu[1], Yuichi Kitamoto[2], Hayato Ouchi[1], Tomonori Ohba[3], Martin J. Hollamby[4], Nobutaka Shimizu[5], Hideaki Takagi[5], Rie Haruki[5], Shin-ichi Adachi[5], Shiki Yagai[1,2]*

Folding one-dimensional polymer chains into well-defined topologies represents an important organization process for proteins, but replicating this process for supramolecular polymers remains a challenging task. We report supramolecular polymers that can fold into protein-like topologies. Our approach is based on curvature-forming supramolecular rosettes, which affords kinetic control over the extent of helical folding in the resulting supramolecular fibers by changing the cooling rate for polymerization. When using a slow cooling rate, we obtained misfolded fibers containing a minor amount of helical domains that folded on a time scale of days into unique topologies reminiscent of the protein tertiary structures. Thermodynamic analysis of fibers with varying degrees of folding revealed that the folding is accompanied by a large enthalpic gain. The self-folding proceeds via ordering of misfolded domains in the main chain using helical domains as templates, as fully misfolded fibers prepared by a fast cooling rate do not self-fold.

INTRODUCTION

Over the past decades, supramolecular polymerization has proven to be a powerful methodology for creating one-dimensional (1D) nanomaterials with interesting stimuli-responsive properties and functions (*1*–*5*). Particularly in the last decade, the knowledge gained from several mechanistic and kinetic studies on their formation process (*6*–*11*) has enabled researchers to prepare supramolecular polymers with controlled chain lengths and molecular weight distribution (*12*–*15*). Despite this progress, current supramolecular polymers still lag far behind biopolymers and even abiotic polymers in terms of higher-order topological complexity and sophistication. Proteins are an epitome of such polymers, for which intricate biological functions are underpinned by well-defined 3D tertiary structures comprising structural domains such as α helices, β sheets, and turns (*16*, *17*). These unrivaled and active topologies are achieved via designed folding processes of sequence-encoded polypeptide chains by cooperative action of various intrachain noncovalent interactions.

Inspired by the remarkable structure-property relationship found in proteins, chemists have developed a variety of abiotic foldamers (*18*, *19*). Although most of these synthetic systems have only secondary structures such as helices, recently, De *et al.* (*20*) have reported success in the rational design of abiotic foldamers that can fold into tertiary structured helix bundles by embedding additional interacting units into their backbones. For supramolecular polymers, however, replicating this folding process to yield higher-order topologies is extremely challenging. The major obstacle lies in the difficulty of incorporating an additional noncovalent interacting site that can guide the folding of the main chains that are also formed noncovalently. Furthermore, most recent supramolecular polymers are based on π-π stacking interactions between extended π-conjugated molecules to provide specific optical and electronic functions (*21*, *22*). Accordingly, these supramolecular polymers have shape-persistent nanostructures with high degrees of internal order (*21*), making it harder to shape their backbones into a higher folded topology.

Here, we report an unprecedented supramolecular polymer system shown by molecule **1**, wherein initially formed misfolded structures are able to self-fold to yield a topology analogous to the tertiary structure of proteins. The supramolecular monomer design in this study is based on our previous observations on barbiturated naphthalene derivatives **2** (*23*) and **3** (*24*) (Fig. 1A). Initially, we discovered that **2** can form uniform toroidal nanofibers via the formation of hydrogen-bonded windmill-shaped hexamers (rosettes) (*25*). As the uniformity of size in the toroids (average radius, 7.6 nm) reflects the generation of "spontaneous curvature" upon stacking of the rosettes with translational and rotational displacements (Fig. 1B) (*26*), we exploited this curvature to engineer continuously curved supramolecular polymers by expansion of the molecular structure to **3** (*24*). Although we obtained helically folded supramolecular polymer fibers that can be converted into misfolded fibers by photoisomerization of **3**, these did not recover the original folded structures by any means other than thermal reconstruction. We infer that the degree of internal order in the supramolecular polymer backbone of **3** is insufficient to reorganize the randomly unfolded structures into the original helically folded structures due to the conformational flexibility of the molecular structure. The degree of internal order of the supramolecular polymer backbone can be improved by, for example, using a more rigid monomer scaffold. This notion ultimately led us to molecule **1** after examining several potential candidates. Folding of supramolecular polymers of **1** proceeds on a long time scale, which enabled us to directly visualize intermediate states of the topological transition using atomic force microscopy (AFM).

RESULTS

Self-folding of supramolecular polymers

Self-foldable supramolecular polymers can be obtained from slowly cooling a methylcyclohexane (MCH) solution of **1** ($c = 5 \times 10^{-6}$ M) from 373 to 293 K at a rate of 1.0 K min^{-1}. Dynamic light scattering

[1]Department of Applied Chemistry and Biotechnology, Graduate School of Engineering, Chiba University, 1-33 Yayoi-cho, Inage-ku, Chiba 263-8522, Japan. [2]Institute for Global Prominent Research (IGPR), Chiba University, Chiba 263-8522, Japan. [3]Graduate School of Science, Chiba University, Chiba 263-8522, Japan. [4]School of Chemical and Physical Sciences, Keele University, Keele, Staffordshire ST55BG, UK. [5]Photon Factory, Institute of Materials Structure Science, High Energy Accelerator Research Organization, Tsukuba 305-0801, Japan.
*Corresponding author. Email: yagai@faculty.chiba-u.jp

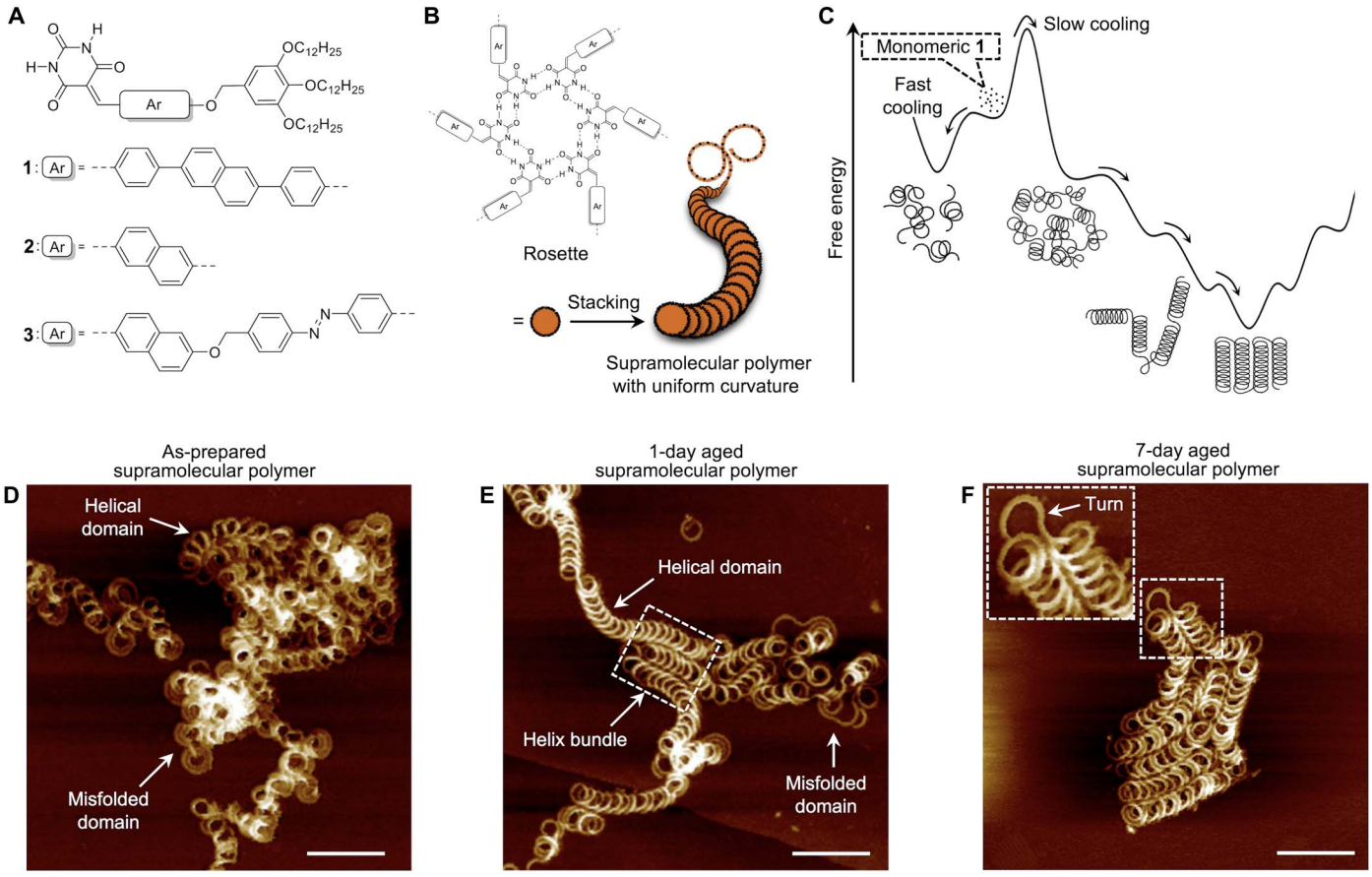

Fig. 1. Self-assembly of barbiturate-substituted molecule into self-foldable supramolecular polymers. (**A**) Molecular structures of barbiturate-substituted π-conjugated molecules **1** to **3**. (**B**) Schematic representation of the curvature-generating supramolecular polymerization of windmill hexamers (rosettes). (**C**) Energy landscape of supramolecular polymers of **1** prepared with fast (left side) and slow cooling (right side). Using a fast cooling rate, a kinetically trapped assembly is formed via isodesmic self-assembly mechanism. Upon slow cooling, misfolded supramolecular polymers containing minor amount of helical domains were initially formed following cooperative nucleation-elongation mechanism, and they slowly transformed into fully folded helical supramolecular polymers via different intermediate, partially folded structures. Black arrows indicate the time evolution processes. (**D** to **F**) AFM images showing the self-folding process of the supramolecular polymers of **1**, which were prepared by cooling a hot MCH solution of **1** ($c = 5 \times 10^{-6}$ M) from 373 to 293 K at a cooling rate of 1.0 K min^{-1}. The samples were spin-coated onto highly oriented pyrolytic graphite (HOPG) substrates after aging at 293 K for 0 min (D), 1 day (E), and 7 days (F). Scale bars, 100 nm. The inset in (F) shows a magnification of the turn segment enclosed by the dashed rectangle.

(DLS) measurements revealed the formation of assemblies with an average hydrodynamic diameter (D_H) of 460 nm. AFM and transmission electron microscopy (TEM) measurements of these assemblies, which were spin-coated from the solution onto appropriate substrates, showed heavily entangled curved fibers (width, ca. 7.7 nm; thickness, ca. 3.5 nm; Fig. 1D and fig. S1). These dimensions are in good agreement with our rosette-based stacking model that induces spontaneous curvature (*24*). The entanglement might be due to the inhomogeneity of the secondary structures involved, as a closer inspection of the individual fibers revealed that most (ca. 60%) of the fiber consists of misfolded conformations, while only a minority (ca. 40%) is present in helically folded conformations. The coexistence of two different secondary structural domains in a single chain suggests that the supramolecular polymerization is kinetically controlled (*27*).

The as-prepared supramolecular polymers involving helical domains slowly self-folded upon aging in solution at 293 K. After 1 day, the fibers were mostly composed of helical domains (>80%) extending up to several hundreds of nanometers (Fig. 1E and fig. S2). Therein, the helical domains were connected by short misfolded segments to afford helix bundles. The self-folding further proceeded over time at higher-order levels, and fully bundled helices, reminiscent of the tertiary structures of proteins, were obtained in quantitative yield after 7 days (Fig. 1F and fig. S3). The helical domains, which exhibited a highly uniform curvature radius (13 ± 1 nm; fig. S4A) and persistent length (170 to 340 nm), were connected by "turn" segments (see inset in Fig. 1F). Preferences for left-handed (*M*) or right-handed (*P*) helices were not observed, and all possible combinations of handedness (*PM*, *MM*, and *PP*) on opposite sides of the turn segments were observed. Further morphological changes, even after prolonged aging, were not observed, which suggests that the system reached the global minimum after 1 week at 293 K via the intermediate structures that constitute local minima in the energy landscape (Fig. 1C).

Small-angle x-ray scattering (SAXS) data of the as-prepared supramolecular polymer solution (Fig. 2A, green curve) exhibited scattering peaks within the range $Q = 0.2$ to 0.9 nm^{-1}. Similar features have previously been ascribed to the spontaneous curvature of the supramolecular polymers (*24*). Here, analysis of the data using a model corresponding to a hollow cylinder (Fig. 2A, dashed curve) gives an

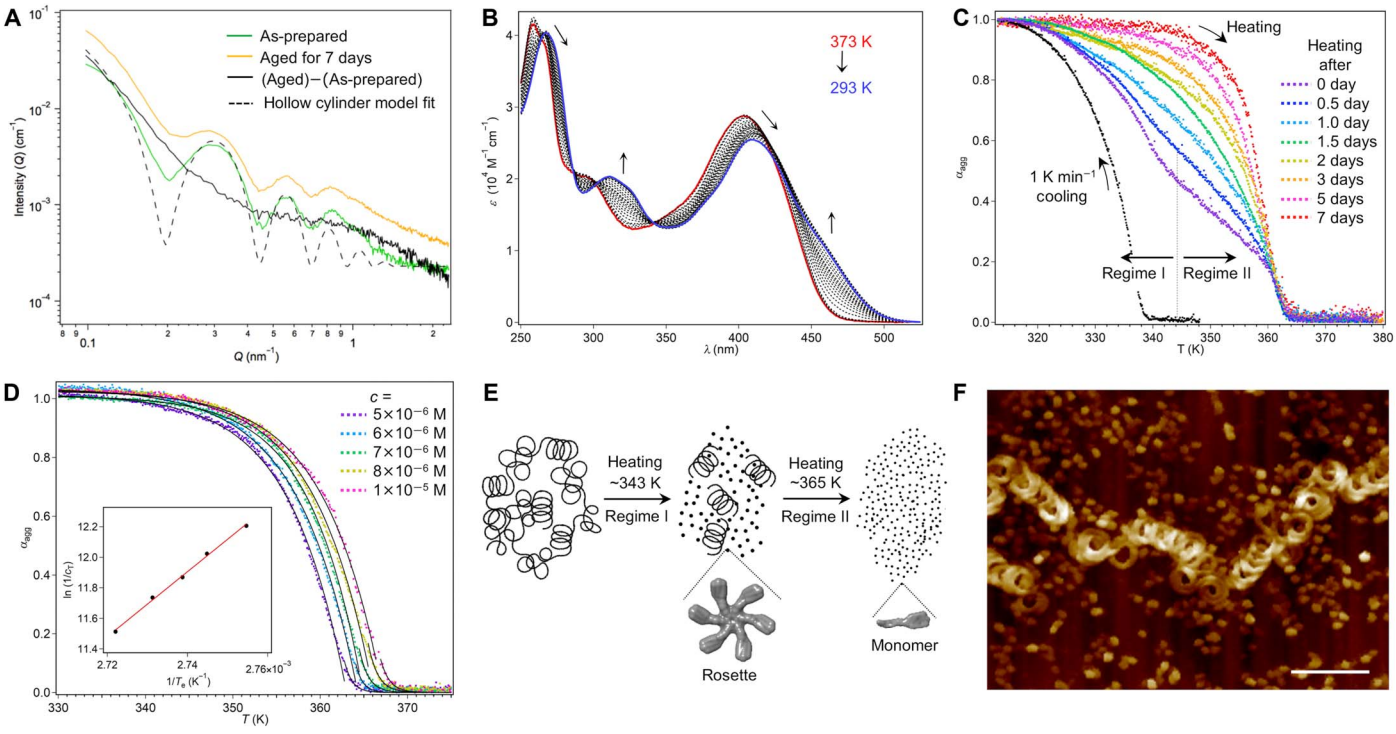

Fig. 2. Dissociation behavior of supramolecular polymers. (**A**) SAXS profiles of the as-prepared solution (green curve) and the 7-day-old solution (orange curve) of **1** ($c = 5 \times 10^{-5}$ M) prepared by cooling from 373 to 293 K at a cooling rate of 1.0 K min^{-1}. The black curve is the profile obtained from subtracting the two data sets. The black dashed curve is a simulation SAXS profile of the as-prepared sample data using a hollow cylinder model. (**B**) Temperature-dependent ultraviolet-visible (UV-Vis) spectra of an MCH solution of **1** ($c = 5 \times 10^{-6}$ M) upon cooling (1.0 K min^{-1}). The arrows indicate the changes in absorption spectra upon cooling. (**C**) Cooling and heating curves of **1** ($c = 5 \times 10^{-6}$ M) in MCH obtained by plotting the molar fractions of the aggregated molecules (α_{agg}, calculated from the absorption change at $\lambda = 470$ nm) as a function of the temperature during cooling (1.0 K min^{-1}; black dots) and subsequent heating after aging for 0 min (purple dots), 12 hours (blue dots), 1 day (cyan dots), 1.5 days (green dots), 2 days (yellow dots), 3 days (orange dots), 5 days (pink dots), and 7 days (red dots) at 293 K. (**D**) Heating curves of the 7-day-old MCH solution of **1**, prepared using a cooling rate of 1.0 K min^{-1} at different concentrations (purple dots, $c = 5 \times 10^{-6}$ M; cyan dots, $c = 6 \times 10^{-6}$ M; green dots, $c = 7 \times 10^{-6}$ M; yellow dots, $c = 8 \times 10^{-6}$ M; pink dots, $c = 1 \times 10^{-5}$ M). The black solid curves were obtained from fitting the experimental data to the cooperative model. Inset: van't Hoff plot obtained from plotting the natural logarithm of c_T^{-1} as a function of T_e^{-1}. The red line shows the corresponding linear fit. (**E**) The proposed mechanism of the thermal dissociation of the as-prepared supramolecular polymer in temperature regimes I and II. (**F**) AFM images of the as-prepared supramolecular polymer of **1**, spin-coated onto HOPG substrate after heating to 343 K for 3 min. Scale bar, 100 nm.

average curvature radius of 12.3 nm, in agreement with the dimensions measured by AFM. After aging (Fig. 2A, orange curve), there is an increase in SAXS intensity throughout the Q range. Subtracting the fresh SAXS data from that collected for the aged sample (Fig. 2A, black curve) gives some insight into the origin of this difference in scattering. As the result is a smooth curve with no observable maxima/minima, it is likely that the SAXS peaks in both samples appear in the same location and have the same magnitude. This in turn suggests that, within this probed size range ($Q = 0.2$ to 0.9 nm^{-1} corresponds to 30 to 7 nm), there is no major change in the structure (that is, it remains, on average, in the coiled state). Also, the subtracted data at $Q < 0.2$ nm^{-1} exhibit a region where $I(Q) \approx Q^{-3}$ and another additional broad contribution centered around $Q = 0.9$ nm^{-1}. Because of limitations of modeling such a complex structure, neither of these features can presently be unambiguously assigned, although the power-law scattering is likely to derive from the more open, equilibrated structures observed by AFM after aging.

Thermodynamic properties of supramolecular polymers

To further corroborate the aforementioned phenomenon, the thermodynamic aspects of the supramolecular polymers at different degrees of folding were investigated by monitoring their thermal dissociation using temperature-dependent absorption spectra. Upon cooling a monomeric solution of **1** ($c = 5 \times 10^{-6}$ M) at a rate of 1.0 K min^{-1}, a new absorption band emerged at ca. 470 nm, which was attributed to π-π stacking of the diphenylnaphthalene cores (Fig. 2B). The growth of this new band showed a nonsigmoidal response to decreasing the temperature, which is characteristic for a cooperative supramolecular polymerization mechanism consisting of nucleation followed by elongation (Fig. 2C, black dots) (*28*, *29*). The critical temperature (T_e) that separates nucleation and elongation was observed at 339 K. Upon heating the as-prepared supramolecular polymer solution (1.0 K min^{-1}), a remarkable thermal hysteresis was observed (*14*, *29*), and the resulting dissociation curve displayed two regimes (I and II) that were separated by an inflection point at ca. 345 K (Fig. 2C, purple dots). In aged solutions, the two regimes became indistinguishable, and cooperative dissociation was observed for solutions aged more than 2 days (Fig. 2C, yellow dots). Equilibration was achieved after 7 days, and the resulting supramolecular polymers dissociated upon heating in a narrow temperature range (ca. 15 K) (Fig. 2C, red dots). A fitting analysis of the equilibrated dissociation curve with a nucleation-elongation model (*30*) provided an elongation enthalpy (ΔH_e) of −171 kJ mol^{-1}

(Fig. 2D, purple dots), which was independent of the concentration (Fig. 2D and table S1A). The quality of the fitting analysis was further validated using a modified van't Hoff plot (see inset in Fig. 2D). Almost identical enthalpy values obtained from the fitting analysis and the van't Hoff plot suggest that the thermodynamic equilibrium is achieved after 7 days (table S1B). The time-dependent absorption measurements showed only a trivial change in molar absorptivity upon folding, suggesting that this process proceeds without altering the molecular arrangement (fig. S5A).

On the basis of the topological changes observed by microscopy techniques, the unusual dissociation curve of the as-prepared solution presumably implies a preferential dissociation of the misfolded domains in temperature regime I due to a lack of the additional enthalpy gain that is expected for the secondary interactions of helical domains along the helix axis (Fig. 2E). Fibers heated at the inflection point showed an apparent decrease of the proportion of misfolded domains under concomitant formation of a large number of uniform 10-nm dots, which were tentatively assigned to isolated or stacked rosettes (Fig. 2F). Accordingly, if supramolecular polymers that are exclusively composed of misfolded domains were prepared, then they should dissociate along a similar trajectory to that of the as-prepared solution in temperature regime I. On the basis of our previous findings, these randomly curved structures should be prepared under highly kinetic conditions such as "quenching" (*7*). We thus cooled a hot solution of **1** ($c = 5 \times 10^{-6}$ M) at a rate of 10 K min^{-1} and obtained fully misfolded supramolecular polymers (Fig. 3, A to D, and fig. S6) with an average D_H of 200 nm. These supramolecular polymers exhibit inhomogeneous curvature radii of 14 ± 4 nm, and their lengths are considerably shorter than supramolecular polymers obtained from slower cooling (1.0 K min^{-1}; fig. S4B). Despite the fact that the absorption features are almost identical to those of the fully folded supramolecular polymers (fig. S5B), the fully misfolded supramolecular polymers dissociated upon subsequent heating, exhibiting a sigmoidal transition, which is characteristic for an isodesmic mechanism (Fig. 3E, red dots) (*29*, *31*). The fully misfolded supramolecular polymers neither self-folded nor showed any evolution of the dissociation curve as a function of time (fig. S7), which is indicative of kinetic trapping (Fig. 1C). A fitting analysis using the isodesmic model (*31*) provided an elongation enthalpy (ΔH_{iso}) of −128 kJ mol^{-1} upon polymerization (Fig. 3E, black curve), which is close to the value of −121 kJ mol^{-1} determined from the corresponding van't Hoff plot (fig. S7, B to E, and table S1C). The strength of π-π stacking interaction should be identical in the fully misfolded and fully folded supramolecular polymers, as evident from their identical absorption spectra. Accordingly, the different elongation enthalpy values obtained for the fully folded supramolecular polymers and fully misfolded supramolecular polymers ($|\Delta H_e - \Delta H_{iso}|$ = 43 kJ mol^{-1}) should be attributed to the presence of van der Waals interactions in the higher-order levels, that is, interactions between loops within a helix to stabilize the secondary structures, and between helices to stabilize the tertiary structures.

Analysis of mechanically fragmented supramolecular polymers

To shed light onto the two aforementioned higher-order interactions, we sonicated a solution of fully folded supramolecular polymers with the expectation that the mechanical stimulus could selectively cleave either interaction. Upon sonication, a decrease in the average D_H of the assemblies was observed (Fig. 4A). AFM images of a sample subjected to sonication for 30 s showed predominantly twin helices (Fig. 4, C to G), which corroborates the fact that the misfolded segments are prone to cleavage. The dissociation curve measured at this stage provided an elongation enthalpy $\Delta H_e'$ of −140 kJ mol^{-1} (Fig. 4B, orange dots). Although twin helices are partially stabilized by interactions between helices, their elongation enthalpy is considerably smaller than that of

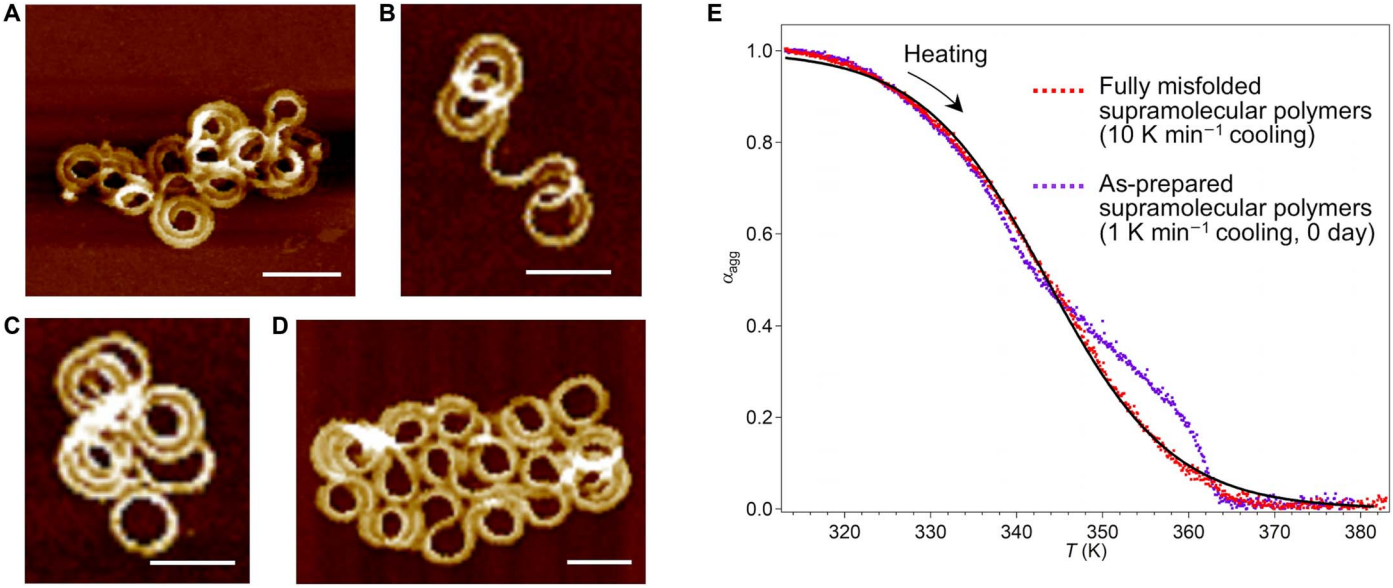

Fig. 3. Misfolded supramolecular polymers. (**A** to **D**) AFM images of fully misfolded supramolecular polymers prepared by cooling a hot solution of **1** ($c = 5 \times 10^{-6}$ M) from 373 to 293 K at a cooling rate of 10 K min^{-1}. The sample was spin-coated onto a HOPG substrate after aging at 293 K for 0 min. Scale bars, 50 nm. (**E**) Heating curve for fully misfolded supramolecular polymers of **1** prepared at a cooling rate of 10 K min^{-1} in MCH (red dots, $c = 5 \times 10^{-6}$ M). The black solid curve was obtained from fitting the experimental data to the isodesmic model. Heating curves for as-prepared supramolecular polymers at a cooling rate of 1.0 K min^{-1} (purple dots; see Fig. 2C) are also shown for comparison.

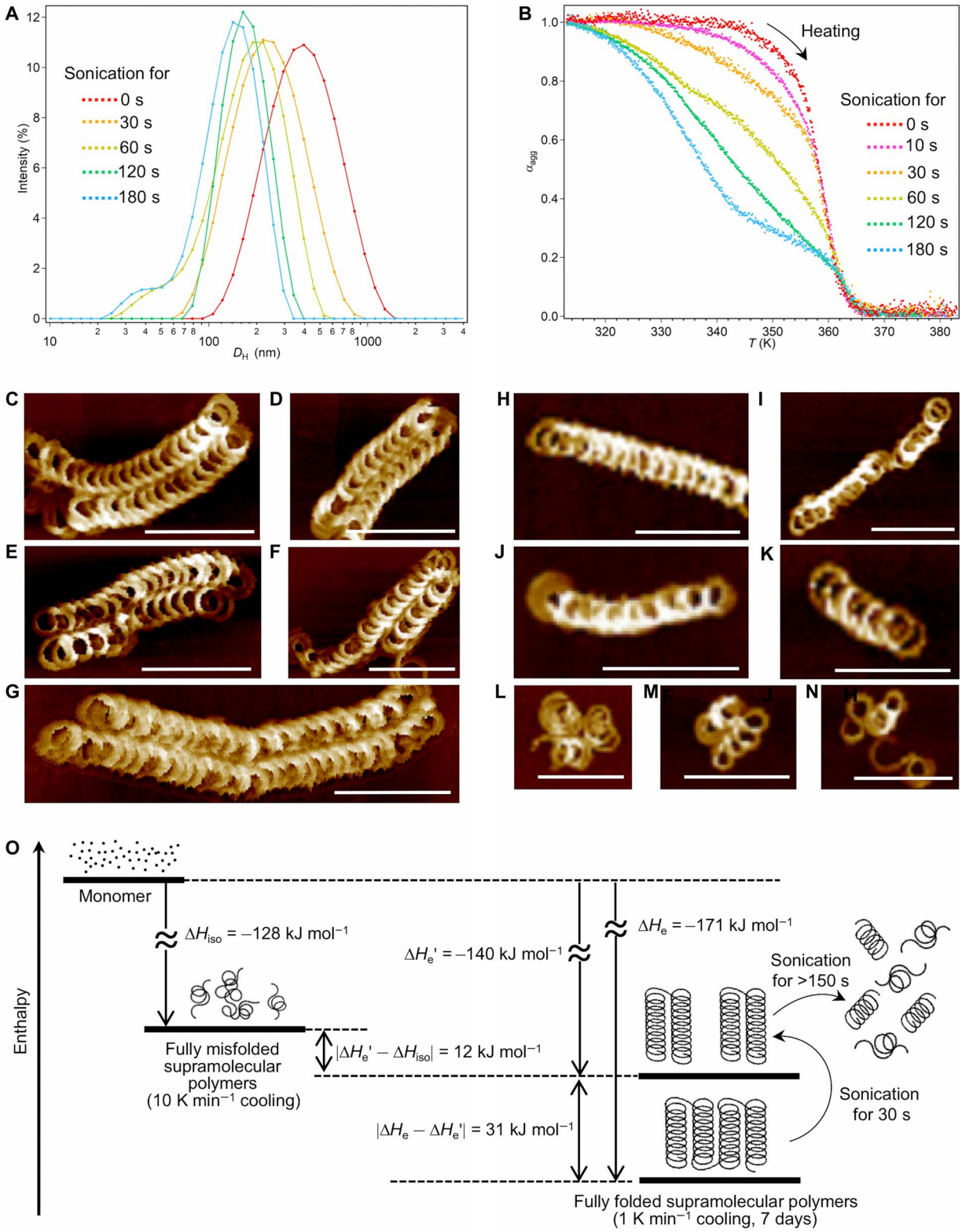

Fig. 4. Mechanically fragmented supramolecular polymers. (**A**) Changes of DLS size distribution of fully folded supramolecular polymers of **1** ($c = 5 \times 10^{-6}$ M) in MCH upon sonication for 0 s (red curve), 30 s (orange curve), 60 s (yellow curve), 120 s (green curve), and 180 s (blue curve) at 293 K. (**B**) Changes in the heating curves upon sonicating the fully folded supramolecular polymer solution of **1** at 293 K for different time intervals (red dots, 0 s; pink dots, 10 s; orange dots, 30 s; yellow dots, 60 s; green dots, 120 s; cyan dots, 180 s). (**C** to **G**) AFM images of twinned helical supramolecular polymers obtained by sonicating the fully folded supramolecular polymers for 30 s. Scale bars, 100 nm. (**H** to **N**) AFM images of single helical supramolecular polymers obtained by sonicating the fully folded supramolecular polymers for 180 s. Scale bars, 100 nm. (**O**) Enthalpy diagram of supramolecular polymers prepared using fast or slow cooling rates and mechanically fragmented supramolecular polymers.

fully folded supramolecular polymers ($|\Delta H_e - \Delta H_e'| = 31$ kJ mol^{-1}) yet closer to ΔH_{iso} of the fully misfolded supramolecular polymers ($|\Delta H_e' - \Delta H_{iso}| = 12$ kJ mol^{-1}; Fig. 4O). These findings illustrate that the interactions between helices contribute predominantly to the stabilization of the fully folded supramolecular polymers.

Further sonication yielded single helices but, at the same time, also fully misfolded supramolecular polymers due to further fragmentation and denaturation of the secondary structure by exposure to the mechanical force (Fig. 4, H to N). The resulting dissociation curve thus exhibited an "inflection point" due to the coexistence of supramolecular polymers with distinct structural conformations (Fig. 4B, cyan dots). The inflected dissociation curve and the morphology of the fragmented supramolecular polymers obtained by sonication did not show any evolution over time. The same observation was made upon mixing supramolecular polymers prepared using cooling rates of 1.0 and 10 K min^{-1}, respectively, followed by aging for 7 days (fig. S8). These results suggest that the fully misfolded supramolecular polymers did not transform into helically folded supramolecular polymers, neither via an external template mechanism nor by a dissociation-reconstruction via the monomer. We thus believe that self-folding occurs only when misfolded and helical domains exist in the same supramolecular polymer chain.

DISCUSSION

An analysis of the AFM images of the as-prepared supramolecular polymers revealed uneven curvature radii in the misfolded domains and a considerably larger deviation (ca. 4 nm) from their average value compared to that in helical domains (ca. 1 nm). The difference implies that the internal order accomplished by a regular stacking of rosettes with translational and rotational displacements is lower in the misfolded domains, and most likely, these domains fluctuate dynamically in solution. In contrast, the helical domains are less dynamic due to a higher degree of internal order and the interactions between loops. Hence, termini of helical domains could act as a "definite curvature template" for the folding of tethered misfolded chains (Fig. 5A), which would lead to secondary helical structures in the first stage of the folding process (ca. 1 day). During the second stage of the folding process (1 to 7 days), two neighboring helical domains, tethered by a misfolded segment, may try to merge into a single helical domain. However, it seems unlikely that termini of the two helical domains that exhibit already-defined curvatures can coalesce while folding the remaining short tether (Fig. 5B, left arrow). It seems more likely that the two helical domains may be folded via a side-by-side contact using the tether segments as a hinge (Fig. 5B, right arrow). If this folding of two neighboring helical domains would occur throughout the supramolecular polymer fibers, then this would lead to tertiary structures. This simple mechanism would be the major reason why our supramolecular polymers self-fold at a very longer time scale compared to natural proteins whose folding proceeds in much shorter period of time (in microseconds) due to covalent local constraints of polypeptide chains and specific intrachain hydrogen bonding. We envisage that similar folded topologies can be more reasonably obtained by designing supramolecular block copolymers composed of different secondary structural domains showing distinct conformational flexibility (for example, ordered static domain and disordered dynamic domain). To produce such copolymers, we have to develop proper methods to join chemically different monomers that can produce distinct domains. Because these monomers are intrinsically prone to self-sort, construction of these unique supramolecular block copolymers is challenging.

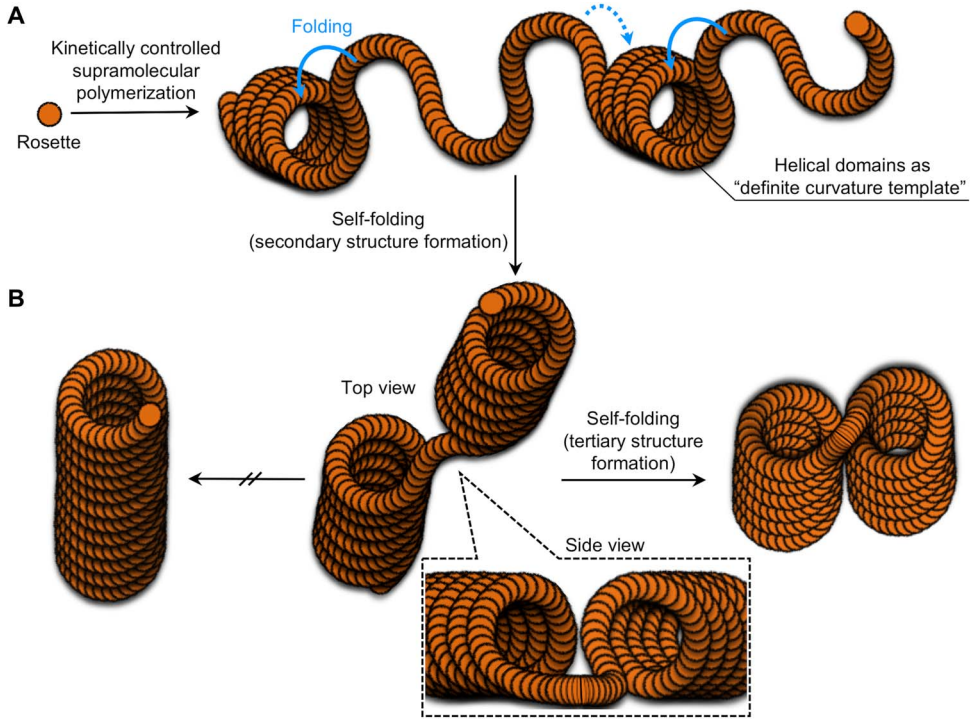

Fig. 5. Proposed mechanism for the self-folding of supramolecular polymers. (**A**) Schematic representation of folding of misfolded domains templated by helical domains to give the secondary structure. (**B**) Schematic representation of the formation of the tertiary structure by folding of helical domains using misfolded segments as "hinge."

MATERIALS AND METHODS

Materials

Compound **1** was synthesized according to the synthetic procedure in the Supplementary Materials. All starting materials and reagents were purchased from commercial suppliers and used without further purification. Air-sensitive reactions were conducted under nitrogen atmosphere using dry solvents. ^{1}H nuclear magnetic resonance (NMR; fig. S9A), ^{13}C NMR (fig. S9B), and high-resolution mass spectrometry (HRMS) details of compound **1** are included in the Supplementary Materials.

General methods

^{1}H and ^{13}C NMR spectra were recorded on Bruker DPS300 and JEOL JNM-ECA500 NMR spectrometers, and chemical shifts were reported in parts per million (δ) with the signal of tetramethylsilane as an internal standard. Electrospray ionization MS spectra were measured on an Exactive mass spectrometer (Thermo Scientific).

UV-Vis spectroscopy

UV-Vis absorption spectra were recorded on a JASCO V660 spectrophotometer equipped with a Peltier device temperature control unit using a screw-capped quartz cuvette of 1.0-cm path length. All the measurements were done while stirring the solution at 500 rpm.

Dynamic light scattering

DLS measurements were conducted on Zetasizer Nano (Malvern Instruments) using noninvasive backscattering (NIBS) technology under 4.0-mW He-Ne laser (633 nm). The scattering angle was set at 173°. A screw-capped quartz cuvette was used for the measurements. The temperature for measurements was kept at 293 K.

Atomic force microscopy

AFM images were obtained under ambient conditions using MultiMode 8 NanoScope V (Bruker Instrument) in Peak Force Tapping (ScanAsyst) mode. Silicon cantilevers (SCANASYST-AIR) with a spring constant of 0.4 N/m and a frequency of 70 kHz (nominal value; Bruker) were used. The samples were prepared by spin-coating (3000 rpm, for 1 min) of MCH solutions (10 μl) of supramolecular polymers aged at 293 K for different time onto freshly cleaved HOPG (5 mm × 5 mm).

Transmission electron microscopy

TEM images were acquired on JEM-2100F (JEOL) at an acceleration voltage of 120 kV. TEM samples were prepared by spin-coating of MCH solutions of supramolecular polymers aged at 293 K for different lengths of time onto a carbon-coated STEM Cu 75P grid (SHR-C075, grade: super ultrahigh resolution carbon; mesh, 339; whole size, 75 μm) and dried under air for 1 hour followed by drying under vacuum for 24 hours.

Small-angle x-ray scattering

SAXS measurements were carried out at BL-10C at the Photon Factory of the High Energy Accelerator Research Organization (KEK) in Tsukuba, Japan (*32*). Solutions were loaded into cells (stainless steel surround, 20-μm-thick quartz glass windows, 1.25-mm path length), and the temperature was maintained at around 293 K (room temperature). An x-ray wavelength of 1.5 Å and a sample-detector distance of 1029 mm (calibrated using silver behenate) gave a detectable Q range of the order of 0.1 to 5.9 nm^{-1}. Sixty frames were collected with an exposure time of 10 s: Radiation damage was not observed, so these data were averaged to give a total integration time of 600 s. The 2D scattering data (detector: DECTRIS PILATUS3 2M) were radially averaged to yield 1D scattering intensity data [$I(Q)$ versus Q]. This was normalized using water as a reference, and the solvent + cell background was subtracted, to give absolute scattering intensity $I(Q)$ in cm^{-1}. All data reduction was carried out using the software package SAngler (*33*).

SAXS data analysis

Basic SAXS analysis was carried out using a model representing hollow cylinders, in line with our previous work (*24*). This approximation is used because, at the present time, there is a lack of tools with which to better analyze the data, in part due to unusual nature of the presented structures. The analysis is carried out solely to demonstrate that the size of the loops obtained via inspection of AFM images can also be verified by SAXS (which presents a bulk average value).

The form factor for a cylinder, with the scattering length density difference between cylinder and solvent Δρ, radius R, and length L, is generally given as follows (*34*)

$$K_{\mathrm{cyl}}(Q,\Delta\rho,R,L,x)=2\pi R^2L\Delta\rho\frac{J_1\left(QR\sqrt{1-x^2}\right)}{QR\sqrt{1-x^2}}\frac{\sin\left({}^{QLx}/_{2}\right)}{{}^{QLx}/_{2}} \quad (1)$$

In Eq. 1, J_1 is the Bessel function of first order. The overall scattering for a delta distribution of hollow cylinders (ΔR = shell width) is then given as

$$I_{\text{hollow cyl}}=N_{\mathrm{cyl}}\int_0^1\Big(K_{\mathrm{cyl}}(q,\rho_{\mathrm{solv}}-\rho_2,R,L,x)+K_{\mathrm{cyl}}(Q,\rho_2-\rho_{\mathrm{solv}},R+\Delta R,L,x)\Big)^2dx \quad (2)$$

In the above, ρ_{solv} and ρ_2 are the scattering length densities of the solvent and the more electron-dense parts of **1**, respectively. Given the approximate nature of the fit, values of $\rho_{\mathrm{solv,model}}=0$ and $\rho_{2,\mathrm{model}}=1\times10^{-6}$ Å^2 were used, with the result that the scaling parameter N includes contributions from both the density of scatterers and the relative scattering length density difference, $((\rho_{2,\mathrm{real}}-\rho_{\mathrm{solv,real}})/1\times10^{-6}\ \text{Å}^2)^2$. Initially, by fixing ΔR at 3.5 nm (based on AFM data), R was obtained using the SASfit analysis software (*34*). Subsequently, an average curvature radius (center to loop center) was calculated as $R+{}^{1}/_{2}\,\Delta R$. Different values of ΔR were trialed (up to ±2 nm), with almost no effect (for example, ±0.1 nm) on the calculated curvature radius.

Analysis of supramolecular polymerization process

The molar fraction of aggregated molecules (α_{agg}) at a certain temperature was calculated from the absorption intensity at λ = 470 nm based on Eq. 3, in which Abs(agg) and Abs(mono) are the absorption intensities of fully aggregated (at the lowest temperature) and purely monomeric states (at the highest temperature), respectively, and Abs(T) is the absorption intensity at a given temperature (T)

$$\alpha_{\mathrm{agg}}=1-\frac{\mathrm{Abs(agg)}-\mathrm{Abs}(T)}{\mathrm{Abs(agg)}-\mathrm{Abs(mono)}} \quad (3)$$

The plot of α_{agg} versus temperature provides heating curves with either nonsigmoidal (cooperative mechanism) or sigmoidal (isodesmic

mechanism) shape, which were fitted using the models proposed by Jonkheijm *et al.* (*30*) (for cooperative mechanism) and Martin (*31*) (for isodesmic mechanism), respectively. The standard values of enthalpy ($\Delta H°$), entropy ($\Delta S°$), and Gibbs free energy ($\Delta G°$) were calculated using the van't Hoff equation.

SUPPLEMENTARY MATERIALS

Supplementary material for this article is available at http://advances.sciencemag.org/cgi/content/full/4/9/eaat8466/DC1

Synthesis and characterization of compounds
Fig. S1. AFM and TEM images of supramolecular polymers before folding.
Fig. S2. AFM and TEM images of supramolecular polymers during folding (1-day aged).
Fig. S3. AFM and TEM images of supramolecular polymers after folding (7-days aged).
Fig. S4. Morphology analysis of supramolecular polymers.
Fig. S5. UV-Vis absorption spectra of supramolecular polymers.
Fig. S6. AFM and TEM images of entirely misfolded supramolecular polymers.
Fig. S7. UV-Vis heating curves of entirely misfolded supramolecular polymers.
Fig. S8. Mixing experiment of fully folded and fully misfolded supramolecular polymers.
Fig. S9. ^{1}H NMR and ^{13}C NMR of **1**.
Table S1. Thermodynamic parameters of supramolecular polymers.
Reference (*35*)

REFERENCES AND NOTES

1. L. Brunsveld, B. J. B. Folmer, E. W. Meijer, R. P. Sijbesma, Supramolecular polymers. *Chem. Rev.* **101**, 4071–4098 (2001).
2. A. Ciferri, *Supramolecular Polymers* (CRC Press/Taylor & Francis, ed. 2, 2005).
3. M. Burnworth, L. Tang, J. R. Kumpfer, A. J. Duncan, F. L. Beyer, G. L. Fiore, S. J. Rowan, C. Weder, Optically healable supramolecular polymers. *Nature* **472**, 334–337 (2011).
4. J. Boekhoven, S. I. Stupp, 25th anniversary article: Supramolecular materials for regenerative medicine. *Adv. Mater.* **26**, 1642–1659 (2014).
5. L. Yang, X. Tan, Z. Wang, X. Zhang, Supramolecular polymers: Historical development, preparation, characterization, and functions. *Chem. Rev.* **115**, 7196–7239 (2015).
6. T. F. A. De Greef, M. M. J. Smulders, M. Wolffs, A. P. H. J. Schenning, R. P. Sijbesma, E. W. Meijer, Supramolecular polymerization. *Chem. Rev.* **109**, 5687–5754 (2009).
7. P. A. Korevaar, S. J. George, A. J. Markvoort, M. M. J. Smulders, P. A. J. Hilbers, A. P. H. J. Schenning, T. F. A. De Greef, E. W. Meijer, Pathway complexity in supramolecular polymerization. *Nature* **481**, 492–496 (2012).
8. M. Kumar, P. Brocorens, C. Tonnelé, D. Beljonne, M. Surin, S. J. George, A dynamic supramolecular polymer with stimuli-responsive handedness for in situ probing of enzymatic ATP hydrolysis. *Nat. Commun.* **5**, 5793 (2014).
9. D. van der Zwaag, P. A. Pieters, P. A. Korevaar, A. J. Markvoort, A. J. H. Spiering, T. F. A. de Greef, E. W. Meijer, Kinetic analysis as a tool to distinguish pathway complexity in molecular assembly: An unexpected outcome of structures in competition. *J. Am. Chem. Soc.* **137**, 12677–12688 (2015).
10. A. Sorrenti, J. Leira-Iglesias, A. J. Markvoort, T. F. A. de Greef, T. M. Hermans, Non-equilibrium supramolecular polymerization. *Chem. Soc. Rev.* **46**, 5476–5490 (2017).
11. S. A. P. van Rossum, M. Tena-Solsona, J. H. van Esch, R. Eelkema, J. Boekhoven, Dissipative out-of-equilibrium assembly of man-made supramolecular materials. *Chem. Soc. Rev.* **46**, 5519–5535 (2017).
12. S. Ogi, K. Sugiyasu, S. Manna, S. Samitsu, M. Takeuchi, Living supramolecular polymerization realized through a biomimetic approach. *Nat. Chem.* **6**, 188–195 (2014).
13. J. Kang, D. Miyajima, T. Mori, Y. Inoue, Y. Itoh, T. Aida, A rational strategy for the realization of chain-growth supramolecular polymerization. *Science* **347**, 646–651 (2015).
14. S. Ogi, V. Stepanenko, K. Sugiyasu, M. Takeuchi, F. Würthner, Mechanism of self-assembly process and seeded supramolecular polymerization of perylene bisimide organogelator. *J. Am. Chem. Soc.* **137**, 3300–3307 (2015).
15. A. Pal, M. Malakoutikhah, G. Leonetti, M. Tezcan, M. Colomb-Delsuc, V. D. Nguyen, J. van der Gucht, S. Otto, Controlling the structure and length of self-synthesizing supramolecular polymers through nucleated growth and disassembly. *Angew. Chem. Int. Ed.* **54**, 7852–7856 (2015).
16. C. Anfinson, Principles that govern the folding of protein chains. *Science* **181**, 223–230 (1973).
17. D. Baker, A surprising simplicity to protein folding. *Nature* **405**, 39–42 (2000).
18. D. J. Hill, M. J. Mio, R. B. Prince, T. S. Hughes, J. S. Moore, A field guide to foldamers. *Chem. Rev.* **101**, 3893–4012 (2001).
19. S. Hecht, I. Huc, *Foldamers: Structure, Properties and Applications* (Wiley-VCH, 2007).
20. S. De, B. Chi, T. Granier, T. Qi, V. Maurizot, I. Huc, Designing cooperatively folded abiotic uni- and multimolecular helix bundles. *Nat. Chem.* **10**, 51–57 (2018).
21. T. Aida, E. W. Meijer, S. I. Stupp, Functional supramolecular polymers. *Science* **335**, 813–817 (2012).
22. S. S. Babu, V. K. Praveen, A. Ajayaghosh, Functional π-gelators and their applications. *Chem. Rev.* **114**, 1973–2129 (2014).
23. S. Yagai, Y. Goto, X. Lin, T. Karatsu, A. Kitamura, D. Kuzuhara, H. Yamada, Y. Kikkawa, A. Saeki, S. Seki, Self-organization of hydrogen-bonding naphthalene chromophores into J-type nanorings and H-type nanorods: Impact of regioisomerism. *Angew. Chem. Int. Ed.* **51**, 6643–6647 (2012).
24. B. Adhikari, Y. Yamada, M. Yamauchi, K. Wakita, X. Lin, K. Aratsu, T. Ohba, T. Karatsu, M. J. Hollamby, N. Shimizu, H. Takagi, R. Haruki, S.-i. Adachi, S. Yagai, Light-induced unfolding and refolding of supramolecular polymer nanofibers. *Nat. Commun.* **8**, 15254 (2017).
25. B. Adhikari, X. Lin, M. Yamauchi, H. Ouchi, K. Aratsu, S. Yagai, Hydrogen-bonded rosettes comprising π-conjugated systems as building blocks for functional one-dimensional assemblies. *Chem. Commun.* **53**, 9663–9683 (2017).
26. M. J. Hollamby, K. Aratsu, B. R. Pauw, S. E. Rogers, A. J. Smith, M. Yamauchi, X. Lin, S. Yagai, Simultaneous SAXS and SANS analysis for the detection of toroidal supramolecular polymers composed of noncovalent supermacrocycles in solution. *Angew. Chem. Int. Ed.* **55**, 9890–9893 (2016).
27. P. A. Korevaar, T. F. A. De Greef, E. W. Meijer, Pathway complexity in π-conjugated materials. *Chem. Mater.* **26**, 576–586 (2014).
28. D. Zhao, J. S. Moore, Nucleation-elongation: A mechanism for cooperative supramolecular polymerization. *Org. Biomol. Chem.* **1**, 3471–3491 (2003).
29. M. M. J. Smulders, M. M. L. Nieuwenhuizen, T. F. A. de Greef, P. van der Schoot, A. P. H. J. Schenning, E. W. Meijer, How to distinguish isodesmic from cooperative supramolecular polymerisation. *Chemistry* **16**, 362–367 (2010).
30. P. Jonkheijm, P. van der Schoot, A. P. H. J. Schenning, E. W. Meijer, Probing the solvent-assisted nucleation pathway in chemical self-assembly. *Science* **313**, 80–83 (2006).
31. R. B. Martin, Comparison of indefinite self-association models. *Chem. Rev.* **96**, 3043–3064 (1996).
32. N. Igarashi, Y. Watanabe, Y. Shinohara, Y. Inoko, G. Matsuba, H. Okuda, T. Mori, K. Ito, Upgrade of the small angle x-ray scattering beamlines at the photon factory. *J. Phys. Conf. Ser.* **272**, 012026 (2011).
33. N. Shimizu, K. Yatabe, Y. Nagatani, S. Saijyo, T. Kosuge, N. Igarashi, Software development for analysis of small-angle x-ray scattering data. *AIP Conf. Proc.* **1741**, 050017 (2016).
34. I. Breßler, J. Kohlbrecher, A. F. Thünemann, SAS fit: A tool for small-angle scattering data analysis using a library of analytical expressions. *J. Appl. Cryst.* **48**, 1587–1598 (2015).
35. V. S. K. Balagurusamy, G. Ungar, V. Percec, G. Johansson, Rational design of the first spherical supramolecular dendrimers self-organized in a novel thermotropic cubic liquid-crystalline phase and the determination of their shape by x-ray analysis. *J. Am. Chem. Soc.* **119**, 1539–1555 (1997).

Acknowledgments

Funding: This work was supported by KAKENHI (grant 26102010) and the Grant-in-Aid for Scientific Research on Innovative Areas "π-Figuration" (grant 26102001) of the Japanese Ministry of Education, Culture, Sports, Science, and Technology (MEXT). This work was performed under the approval of the Photon Factory Program Advisory Committee (proposal no. 2016G550). S.Y. acknowledges financial support from the Nagase Science and Technology Foundation. **Author contributions:** S.Y. and D.D.P. conceptualized the project. D.D.P. performed most of the experiments described in the study including the synthesis of molecule **1**. N.S., H.T., R.H., and S.-i.A. collected SAXS data. M.J.H. simulated the SAXS data and wrote the "Small-angle x-ray scattering" section of the article. T.O. performed the TEM experiments. D.D.P. and S.Y. wrote the overall manuscript. S.Y. and D.D.P. worked on the figures. All authors including K.A., Y.K., and H.O. commented on the manuscript. The overall project management was by S.Y. **Competing interests:** The authors declare that they have no competing interests. **Data and materials availability:** All data needed to evaluate the conclusions in the paper are present in the paper and/or the Supplementary Materials. Additional data related to this paper may be requested from the authors.

Submitted 10 April 2018
Accepted 27 July 2018
Published 7 September 2018
10.1126/sciadv.aat8466

Citation: D. D. Prabhu, K. Aratsu, Y. Kitamoto, H. Ouchi, T. Ohba, M. J. Hollamby, N. Shimizu, H. Takagi, R. Haruki, S.-i. Adachi, S. Yagai, Self-folding of supramolecular polymers into bioinspired topology *Sci. Adv.* **4**, eaat8466 (2018).

Science Advances

Self-folding of supramolecular polymers into bioinspired topology

Deepak D. Prabhu, Keisuke Aratsu, Yuichi Kitamoto, Hayato Ouchi, Tomonori Ohba, Martin J. Hollamby, Nobutaka Shimizu, Hideaki Takagi, Rie Haruki, Shin-ichi Adachi and Shiki Yagai

Sci Adv **4** (9), eaat8466.
DOI: 10.1126/sciadv.aat8466